We are IntechOpen, the world's leading publisher of Open Access books Built by scientists, for scientists

4,800
Open access books available

122,000
International authors and editors

135M
Downloads

Our authors are among the

154
Countries delivered to

TOP 1%
most cited scientists

12.2%
Contributors from top 500 universities

CLARIVATE ANALYTICS BOOK CITATION INDEX INDEXED

WEB OF SCIENCE™

Selection of our books indexed in the Book Citation Index in Web of Science™ Core Collection (BKCI)

Interested in publishing with us?
Contact book.department@intechopen.com

Numbers displayed above are based on latest data collected.
For more information visit www.intechopen.com

10

Wavelet Transform for Electronic Nose Signal Analysis

Cosimo Distante[1], Marco Leo[1] and Krishna C. Persaud[2]
[1]*Consiglio Nazionale delle Ricerche – CNR*
[2]*University of Manchester*
[1]*Italy*
[2]*United Kingdom*

1. Introduction

Semiconductor gas sensors have been studied for many years and they are now used in many fields of application. Despite this wide trade further research needs mainly to improve sensitivity, selectivity and stability. In fact, in this sense, improving both, the sensor selectivity toward specific gaseous substances and discrimination capability, has been the goal of a great deal of work over the last few years. One strategy consists of using non selective sensor arrays and an appropriate pattern recognition system capable of recognizing simple or complex vapors based on the conductance or current at the saturation point of each transient response. We believe that most useful information (high and low frequencies in the curve) can be taken from the transient response. One of the most important processing part of an intelligent system, is its ability to extract useful information less redundant than the original one to aid fast processing and pattern classification. In other words: any selected feature (1) must discriminate clearly between two or more classes of objects, (2) must not be correlated with another feature to any moderate strong extent, and (3) should have meaning for humans. The first step toward the pre-processing of e-nose data was based on methods for extracting information of the transient only from the steady-state and baseline response values. However, these methods takes into account only stationary information about the transient (i.e. steady-state and baseline) but all the information related to the kinetic of the rise and recovery time is lost. Each sensor has its own behavior in response to an odor presentation that is stored along the response. For example, starting from the fact that light molecules (i.e. alcohol) get more dispersed than heavier one (i.e. acid oils), it is possible to analyse the recovery time of the response due to the end of the exposure to recognize the odor being presented. In some cases of long time sensor response (of the order of several minutes), it is possible to analyse the rise time of the transient response that can be computed in a few seconds instead of considering the saturation parameters.

The common problem encountered with electronic nose applications is the non-reproducibility of sensor responses over time due to drift effects. Drift is a slow change in sensitivity that occur in time due to ageing effects, slow morphological changes in the sensor material, poising and other long- term effects.

The instability of sensor responses could be connected to morphological evolution of the sensing material, so that it is needed to age the sensors for several weeks in the laboratory

bench test before their use. However long term drift is more associated with the contamination of the sensor material due to presence of atmospheric pollution that irreversibly react on sensor surface leading to a reduction of sensitivity.
Pijolat et al. (2003) proved that the presence of a very low concentration of SO_2 in environment can be at the origin of the tin dioxide sensor drift. In this case the problem was overcome by pre-treated the sensors in SO_2 before their use. Such a gaseous treatment had been used in the past to improve the stability of sintered tin dioxide sensor, especially with respect to effect of humidity. This type of treatment can be used with other gases if there is a clear view of the mechanism of interaction between the sensing layer and the gases. Unfortunately all processes concerning drift are not yet well known and the sensor instability depends upon time-varying parameters such as the historical use of the sensors, interactions with several volatile compounds present in the environment at various concentrations, the exposure period to certain substances. Actually a great deal of work has been directed towards the development of methods to minimize the drift effects Sisk & Lewis (2005). An efficient approach could be to use a continuous re-calibration for the training phase of the pattern recognition model, but in the real applications the use of sets of samples for the calibration is very expensive and time-consuming, which makes it unlikely to re-calibrate the pattern recognition model very often. Attempts for drift minimizing have been made by using a reference gas as a reference value and then correcting all subsequent readings accordingly Haugen et al. (2000). Component correction is a method using one or more reference gases. This linear method is based on PCA and PLS algorithms and removes the drift direction calculated from measurements of a reference gas Artursson et al. (2000). The technique use a linear model and has been used at feature level. Multiple Self-Organizing Maps (MSOM) has been developed in Distante, Sicilian & Persaud (2002) because new recognized data that match the stored recognized odors can be continuously used to retrain the classifier. This technique has the advantage of having self-recalibration mechanisms without the intervention of a user. However, the drift must be gradual, as a discontinuity in response between consecutive exposures (regardless of the time interval between the exposures) would immediately invalidate the classification model and would prevent adaptation Sisk & Lewis (2005). Others drift counteracting methods focus on the application of signal pre-processing techniques to filter out portions of the signal containing drift contaminations. Drift is in general a time scale longer than the duration of a single measurement, thus a selection of the lowest frequency components of the sensor responses are needed to filter it out.
A moving median filter and Fourier band-pass filters are some examples of filters applied to removing either high-frequency fluctuations (such as noise, spikes) or low-frequency changes such as drift. In comparison to these filters, Discrete Wavelet Transform (DWT) technique provides a flexible analysis of the signal at different resolutions by applying iteratively high-pass and low-pass filters Bakshi (1999); **?**. Therefore the wavelet transform is a powerful tool to point out drift contamination in the low-frequency behavior of the sensor responses. As it is shown in this paper, this technique allows to remove the selected low-frequency components easily and in such a way that the signal is not distorted. The comparison of the DWT filter and others commonly used have been compared with the relative method feature extraction technique which is commonly used in this context. Principal component analysis shows than that DWT approach is superior in terms of cluster dispersion. The DWT is here also ebmedded into MSOM neural network Distante, Sicilian & Persaud (2002); Zuppa et al. (2007) as it is able to detect and adapts to clusters trend Zuppa et al. (2004). The use of

smoothing filters as the Savitzky-Golay and Discrete Wavelet Trasform on this function allows to cut off the frequency components which do not influence its behaviour.

2. Related works

There has been a lot of work in using discrete wavelet trasform for electronic nose data since our initial paper in Distante, Leo, Siciliano & Persaud (2002). Since the interesting information resides in low frequency components as will be shown below, all the referenced works of DWT for electronic noses make use of the approximation coefficients which are the results of the low-pass filter with the analysing signal. In this case, approximation coefficients allows for signal representation, where there should be made distinction when extracting features for classification or compression tasks. Both tasks demand for signal simplification Rubinstein et al. (2010), but in Leone et al. (2005) it has been shown that for classification purposes, the fewer the number of decriptors, the better the accuracy. In Phaisangittisagul & Nagle (2008) features are extracted from the transient with discrete wavelet transform (DWT) in order to search for an optimal sensor array to be implemented in the e-nose system. Two different odor datasets such as coffee and soda are collected and a genetic algorithm is adapted to tailor a gas sensor array. Two different mother wavelets were used: Haar and Daubechies of second order ($db2$). Several decomposition levels were investigated, Haar third level and $db2$ at third fourth and fifth. As expected, Haar provide lower classification performance with respect to $db2$. The fifth decomposition level (approximation coefficients) has been selected and given to the $k-Nearest-Neighbor$ classifier. In Phaisangittisagul & Nagle (2010) a signal decomposition/reconstruction based on the discrete wavelet transform is proposed, whose coefficients are given to a support vector regression to predict a sensor's response to mixtures of odors. Prediction is performed on different mixing ratios of Regular, Sumatra coffees and Grean tea components. The idea is to predict sensor response by starting from the mixing ratios. Wavelet coefficients (both approximationa and details) have been used to train support vector regression (SVR) machines to predict the respective coefficients at lower level going backward for inverse discrete wavelet trasform to reconstruct the signal. So far, for each decomposition level, two SVR's (one for approximation coefficients and one for details) are trained. SVR parameters have been found using an optimization technique based on genetic algorithm. The considered sensor for the response prediction study is a MOSFET 101A sensor of the NST 3320 e-nose. The highest decomposition level must be manually chosen, where the 5th level has shown to be the most appropriate for the probelm at hand. Infact, choosing lower scales brings to the overfitting problem by loosing generalization capabilities, while going to higher scales increase the predicted error since it accumulates with the number of decomposition levels along the reconstruction process with IDWT. A study of the number of extracted features for the classification of several volatiles have been investigated in Acevedo et al. (2007). They show the number of coefficients needed to reach optimal classification accuracy with techniques such as: DWT, DCT, PCA and linear discriminant analysis (LDA).
The ability of the DWT to recover sensor signals subjected to *drift* effects has been addressed in Huang & Leung (2009); Zuppa et al. (2007). The drift, such as the seasonal fluctuation, resides in low frequencies. Wavelet analysis is used, in order to decompose the drifting signal at the greatest scale value to reveal signal trend. The trend is the slowest part of the signal and as the scale increases a better estimate of the unknown trend is obtained. So far, DWT is an efficient tool for pre-processing drifting sensor responses as it allows to select and discard signal components, where drift contamination is present, without distorting the signal by

excessive cutting off low-frequency components. The results are compared with ones obtained by applying usual high-pass filters.
The use of DWT for tin dioxide gas sensor has also been investigated on a robotic platform Trincavelli et al. (2009) in a continuos sampling setup. The plume to be tracked can be generated by ethanol, acetone or isopropyl. A feature vector composed on a combination of DWT, curve fitting and discrete Fourier Transform coefficients have been considered and provided to an SVM classifier. Similarly, in Loutfi et al. (2009) a mobile platform is used to integrate classification of odours with gas distribution mapping. The resulting odour map is then correlated with the spatial information collected from a laser range scanner to form a combined map. Two electronic noses are present onboard based on TGS Figaro technology. Each e-nose consists of four TGS sensors (TGS 2600 (ÃŮ2), 2620, 2602). A temporal analysing window of 20-30 seconds of measurements are considered for the classification task. Signals goes DWT analysis whose coefficients are projected onto the first two proncipal components (PCA). Then SVM is used to classify between ethanol, acetone and air.

3. Wavelet analysis

Wavelet transform is an extension of Fourier Transform, generalized to any wideband transient. Let us think to our input as a time-varying signal. To analyze signal structure of very different sizes, it is necessary to use time-frequency atoms with different time support. The wavelet transform decomposes signals over dilated and translated wavelets Mallat (1999). The signal may be sampled at discrete wavelength values yielding a spectrum. In continuous wavelet transform the input signal is correlated with an analyzing continuous wavelet. The latter is a function of two parameters such as scale and position. The widely used Fourier transform (FT) maps the input data into a new space, the basis functions of which are sines and cosines. Such basis functions are defined in an infinite space and are periodic, this means that FT is best suited to signal with these same features. The Wavelet transform maps the input signal int a new space, the basis function that are quite localized in space. They are usually of compact support. The term *wavelet* comes from well localized wave-like functions. Infact, they are well localized in space and frequency i.e. their rate of variations is restricted. Fourier transform is not local in space but only in frequency. Furthermore, Fourier analysis is unique, but wavelet not, since there are many possible sets of wavelets which one can choose. Our trade-off between different wavelet sets is compactness versus smoothness.
Working with fixed windows as in the Short Term Fourier Transform (STFT) may bring to problems. Infact, if the signal details are much smaller than the width of the window they can be detected but the transform will not localize them. If the signal details are larger than the window size, then they will not be detected properly. The scale is defined by the width of a modulation function. To solve this problem we must define a transform independent from the scale. This means that the function should not have a fixed scale but should vary. To achieve this, we start from a function $\psi(t)$ as a candidate of a modulation function and we can obtain a family starting from it by varying the scale s as follows:

$$\psi_s(u) = |s|^{-p}\psi(\frac{u}{s}) = \frac{1}{|s|^p}\psi\left(\frac{u}{s}\right) \quad p \geq 0 \quad \forall s \in \Re \quad s \neq 0. \tag{1}$$

If ψ has width T then the width of ψ is sT. In term of frequencies, we can state that small scales s implies ψ_s has high frequencies and increasing s the frequency of ψ_s decreases.

3.1 Continuous wavelet transform

As it is well known, FT uses basis functions consisting of sines and cosines functions. These functions are time-independent. Hence, the description of a signal provided by Fourier analysis is purely in the frequency domain. The windowed Fourier transform and the wavelet transform aims at the analysis of time and frequency. For non-stationary analysis, a windowed Fourier transform or Short Time FT (STFT) is best suited. The smaller the window size the more the number of discrete frequencies that will be reduced, leading to a weak discrimination potential among frequencies. Given a signal $f(t)$, a window g around the time-point τ and frequency ω is

$$STFT(\tau,\omega) = \int_{-\infty}^{+\infty} f(t)g(t-\tau)e^{-j\omega t}dt. \tag{2}$$

Now considering

$$k_{\tau,\omega}(t) = g(t-\tau)e^{-j\omega t} \tag{3}$$

as a new basis and rewriting this with window s inversely proportional to the frequency ω and the position parameter b that replaces τ gives the following

$$k_{b,s}(t) = \frac{1}{\sqrt{s}}\psi^*\left(\frac{t-b}{s}\right) \tag{4}$$

that yields to the continuous wavelet transform (CWT).
While in STFT the basis functions are sinusoids, in the CWT they are scaled versions of the so called mother wavelet ψ (ψ^* represents the conjugate i.e. $\psi_s^*(u) = \frac{1}{\sqrt{s}}\psi(-\frac{u}{s})$. A wavelet mother function can be constructed in several ways, but subjected to admissibility constraints.

Definition The Morlet-Grossman definition of the continuous wavelet transform for a 1-dimensional signal $f(t) \in L^2(\Re)$,the space of all square integrable functions, is given as follows:

$$\tilde{f}(a,b) = \frac{1}{\sqrt{a}}\int_{-\infty}^{+\infty} f(t)\psi^*\left(\frac{t-b}{a}\right)dt \tag{5}$$

where:

- $Wf(a,b)$ is the wavelet coefficient of the function $f(t)$,
- $\psi(t)$ is the mother wavelet,
- $a > 0$ is the scale parameter,
- b is the position parameter.

We can also rewrite eq. 5 as a convolution product:

$$\tilde{f}(a,b) = f \star \psi_s(t). \tag{6}$$

The continuous wavelet transform is the result of the scalar product of the original signal f with the *shifted* and *scaled* version of a prototype analysing function $\psi(t)$ called *mother wavelet* which has the characteristic of a bandpass filter impulse response. The coefficients $\tilde{f}$ of the transformed signal f represent how closely correlated the mother wavelet is with the section of the signal being analyzed. The higher the coefficient is, the more the similarity[1].
The continuous wavelet transform has the following properties:

1. CWT is a linear transformation,
2. CWT is covariant under translation,
3. CWT is covariant under dilation.

[1] Note that the result will depend on the shape of the wavelet you choose.

3.2 Wavelet functions

As it is know, to analyse signals of very different sizes, it is necessary to use time-frequency atoms with different time support. A wavelet $\psi \in L^2(\Re)$ is a function with a zero average

$$\int_{-\infty}^{+\infty} \psi(t)dt = 0, \tag{7}$$

and is also normalized $\|\psi\| = 1$ and centered in the neighborhood of $t = 0$. The scaled and translated versions $\psi_s(u)$ remain normalized as well.

3.2.1 Haar wavelet

In 1910, Haar realized that one can construct a simple piece-wise constant function as shown in figure 1a and is defined as follows:

$$\psi(t) = \begin{cases} 1 \; if \;\; 0 \leq t < 1/2 \\ -1 \; if \;\; 1/2 \leq t < 1 \\ 0 \quad otherwise \end{cases} \tag{8}$$

whose dilation and translations generate an orthonormal basis of $L^2(\Re)$.
Application of this transform to data smoothing and periodicity detection

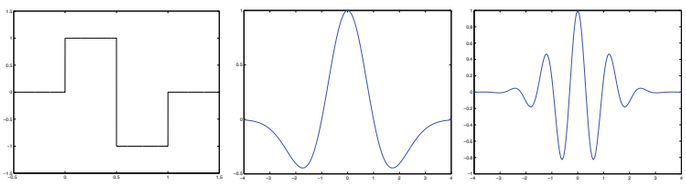

(a) (b) (c)

Fig. 1. Mother wavelet functions: (a) Haar, (b) Mexican hat and (c) Morlet.

3.2.2 Mexican hat

The Mexican hat is the second derivative of a Gaussian (see fig. 1b)

$$g(t) = (1 - t^2)e^{-t^2/2} \tag{9}$$

They were first used in computer vision to detect multiscale edges.

3.2.3 Morlet's wavelet

This wavelet is defined as follows

$$g(v) = e^{2\pi^2(v-v_0)^2} \tag{10}$$

which is shown in fig. 1c

3.3 Discrete wavelet transform

Calculating wavelet coefficients at every possible scale is a fair amount of work, and it generates an awful lot of data. What if we choose only a subset of scales and positions at which to make our calculations?
It turns out, that if we choose scales and positions based on power of two (called *dyadic* scales and positions) then our analysis will be much more efficient. This analysis is called the *discrete wavelet transform*.

In the discrete case, WT is sampled at discrete meshpoints and using smoother basis functions. But, how to discretize the time-scale domain in order to have a discrete wavelet transform (DWT)?
In the windowed Fourier transform the time frequency domain was discretized using a uniform lattice $\Delta(t_0, \omega_0) = \{(mt_0, n\omega_0)|m, n \in Z\}$ where t_0 and ω_0 are the time and position respectively.
It is known that scaling operation acts as a multiplicative way, that is, composing two consecutive scaling is attained by multiplying each of the scale factor. Thus, starting from an initial scale $s_0 > 1$ we consider all the discrete scales

$$s_m = s_0^m \quad m \in Z \tag{11}$$

Now, how to discretize the time? It is important to note that we must obtain a lattice in the time-scale domain in order to sample (with a minimum redundancy reconstruction of the original signal) the continuous wavelet transform we have seen before from the time-scale domain $\tilde{f}_{m,n}$.
Changing the scale, results in the increase of the width of the wavelet. Also, when the width of the wavelet reduces with a scale reduction operation, we must increase the frequency. One of the most important properties of the WT is the invariance under scale changes. Infact, if we change the scale in the function f and the scale of the underlying space by the same scaling factor, the WT does not change. If we take $f_{s_0}(t) = s_0^{-1/2} f(t/s_0)$ this implies $\tilde{f}_{s_0}(s_0 s, s_0 t) = \tilde{f}(s, t)$.
The invariance property of the wavelet transform is very important and should be preserved even when the WT is discretized. The preservation can be accomplished when we pass from one scale $s_m = s_0^m$ to the other $s_{m+1} = s_0^{m+1}$ by incrementing the time by the scaling factor s_0. We can choose an initial time t_0 and take the length of the sampling time intervals $\Delta t = t_0 s_0^m$. The time discretization lattice for each scale s_0^m is given by

$$t_{m,n} = n s_0^m t_0 \quad n \in Z \tag{12}$$

and the time-scale discretization domain in the lattice is

$$\Delta_{s_0,t_0} = \{(s_0^m, n s_0^m t_0)|m, n \in Z\} \tag{13}$$

the discretization of the WT $\tilde{f}(s, t) =< f, \psi_{s,t}(u) >$ in the time scale lattice is given by

$$\tilde{f}_{m,n} =< f, \psi_{m,n}(u) > \tag{14}$$

where

$$\psi_{m,n}(u) = s_0^{-m/2} \psi(s_0^{-m} u - n t_0). \tag{15}$$

The discrete WT has the following characteristics:

- the sequence $< f, \psi_{m,n} > \quad m, n \in Z$ is an exact representation of f,
- it is possible to reconstruct f from the family of wavelet time-scale atoms $\psi_{m,n}$,
- $\{\psi_{m,n}\}$ constitutes an orthonormal basis for $L^2(\Re)$.

3.4 Multiresolution and subband coding

In the previous sections we have seen the continuous wavelet transform and its discretization in the time-scale domain.

The idea of the scale is mainly related to the problem of point sampling of the signal. When we sample a signal, we have to fix the sampling frequency[2] and the sampling period[3]. If we are sampling the signal at a frequency 2^j this means that frequencies (*details*) outside the scale magnitude of the samples will be last in the sampling process. All of the details captured in a certain scale, will be present at higher scales $2^k \;\; k > m$.

The scaling process gives rise to a subspace generation. Infact, sampling with a frequency of 2^j can give rise to the formation f the subspace $V_j \in L^2(\Re)$ which is constituted by the functions in $L^2(\Re)$ whose details are well represented in the scale 2^j. Now let us define a representation operator that will represent the function $f \in L^2(\Re)$ in the scale 2^j. Let us suppose that there exist a function $\phi \in L^2(\Re)$ such that the family of functions

$$\phi_{j,k}(u) = 2^{-j/2}\phi(2^{-j}u - k) \quad j,k \in Z \tag{16}$$

that represent an orthonormal basis for the subspace V_J.

Defining different scales of ϕ we have

$$\phi_s(u) = \frac{1}{|s|^{1/2}}\phi(\frac{u}{s}) \tag{17}$$

where the width of ϕ is s-times the width of ϕ_s. Thus, as the scale increases or decreases the width of ϕ_s does the same. Now taking $s = 2^j \; j \in Z$ we have

$$\phi_{j,k} = \phi_{2^j}(u - k) = 2^{-j/2}\phi(2^{-j}u - k) \tag{18}$$

is an orthonormal basis for V_j.

For each space V_j with scale 2^j we can define the operator $R_j : L^2(\Re) \rightarrow V_j$. This represent the representation operator that orthogonally project a function $f \in L^2(\Re)$ in the space V_j as follows

$$R_j(f) = Proj_{V_j}(f) = \sum_k < f, \phi_{j,k} > \phi_{j,k}. \tag{19}$$

From the previous relationships emerges that we can represent a function f at several scales. It is important to change the representation from one scale to another without loosing information. The details of one scale at 2^j must appear at a smaller scale 2^{j-1}. Thus $V_j \in V_{j-1}$ that means: given a function $f \in L^2(\Re)$ then $f \in V_j$ iff $f(2u) \in V_{j-1}$ and recursively we can obtain the following

$$f \in V_j \quad iff \quad f(2^j u) \in V_0 \tag{20}$$

Let us now define the multiresolution representation as follows

Definition A multiresolution representation in $L^2(\Re)$ is defined as a sequence of closed subspaces $V_j \in L^2(\Re) \; j \in Z$ that satisfies the following properties:

1. $V_j \subset V_{j-1}$
2. $f \in V_j$ iff $f(2u) \in V_{j-1}$

[2] The number of samples in the time unit.

[3] The length of the sample interval.

3. $\bigcap_{j\in Z} V_j = \{0\}$
4. $\bigcup_{j\in Z} V_j = L^2(\Re)$
5. $\exists\phi \in V_0 \ni' \{\phi(u-k)|k \in Z\}$ is an orthonormal basis of V_0.

The function ϕ is called the *scaling function* of the multiresolution representation. Each of the spaces V_j is called *scale spaces*, or, more precisely, space of scale 2^j.
The orthogonal projection of $f \in L^2(\Re)$ in the space V_j is obtained by using a filtering process of f with the different kernels $\phi_{j,k}\ k \in\ Z$ which define low-pass filters. Defining the Haar multiresolution representation as

$$\phi(t) = \begin{cases} 0\ if\ \ t < 0\ \ and\ \ t \geq 1 \\ 1 \qquad if\ \ t \in [0,1) \end{cases} \tag{21}$$

whose family represents basis function of the subspace

$$V_j = \{f \in L^2(\Re); f[2^j k, 2^j(k+1)] = constant, k \in Z\}. \tag{22}$$

That is the projection of f on the scale space V_j is given by a function that is constant in the interval $[2^j k, 2^j(k+1)]$. Thus the orthogonality projection of $f \in L^2(\Re)$ in the space V_j is obtained using a filtering process of f with the different kernels $\phi_{jk}\ k \in Z$ which define low-pass filters.
Let us now interpret geometrically the sequence of nested scale spaces in a multiresolution representation. Indicating the cutting frequency α_j of this filters we can say that the space V_j is constituted of functions whose frequencies are contained in the interval $[-\alpha_j, \alpha_j]$, $\alpha_j > 0$. Going to a finer scale V_{j-1} we change to the interval $[-\alpha_{j-1}, \alpha_{j-1}]$, where the relation of the two subspaces V_j and V_{j-1} is given by

$$V_{j-1} = V_j \star W_j \tag{23}$$

where W_j is the *detail space* that comprises all the functions of $L^2(\Re)$ with frequencies in the band $[\alpha_j -, \alpha_{j-1}]$ of the spectrum. Thus W_j is orthogonal to V_j and the above states that a function represented on a finer scale space V_{j-1} is obtained from the representation on a coarser scale space V_j by adding details W_j. The details can be obtained by projecting a function f in each subspace W_j using band-pass filtering whose pass-band is exactly $[\alpha_j -, \alpha_{j-1}]$. In fact, this filtering process can be computed by projecting f on an orthogonal basis of wavelets. For each $j \in Z$ there exists an orthonormal basis of wavelets $\{\psi_{j,k}, k \in Z\}$ of the space W_j. Therefore, if R_j is the representation operator on the scale space V_j, we have, for all $f \in L^2(\Re)$

$$R_{j-1}(f) = R_j(f) + \sum_{k\in Z} < f, \psi_{j,k} > \psi_{j,k}. \tag{24}$$

The second term represent the orthogonal projection of function f on the space W_j and it will be denoted by $Proj_{W_j}(f)$. Now rewriting eq. 23 in terms of filters we have

$$R_{j-1}(f) = R_j(f) + Proj_{W_j}(f) R_{j-2}(f) = R_{j-1}(f) + Proj_{W_{j-1}}(f) ... \tag{25}$$

iterating this equation for $R_{j-2}, ..., R_{j-J_0}$, summing up both sides and performing the proper cancellations, we obtain

$$R_{j-J_0}(f) = R_j(f) + Proj_{W_{j-1}}(f) + ... + Proj_{W_{j-J_0}}(f). \tag{26}$$

The projection $R_j(f)$ represents a version of low resolution (*approximation*) of the signal obtained using successive low-pass filters $\phi_j, \phi_{j-1}, ..., \phi j - J_0$. The terms $Proj_{W_{j-1}}(f), ..., Proj_{W_{j-J_0}}(f)$ represent the *details* of the signal lost in each low-pass filtering. This details are obtained by filtering the signal using the wavelets $\psi_j, \psi_{j-1}, ..., \psi j - J_0$.

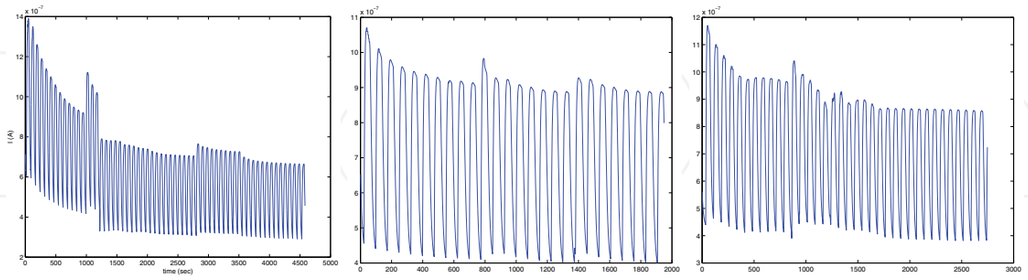

Fig. 2. Three responses relative to Pentanone, Acetone, and Exanal in 50%RH (from left to right).

4. Experiments

4.1 DWT analysis

The active layers of the array consist of pure and doped SnO_2 thin films prepared by means of sol-gel technology. Pd, Pt, Os, and Ni were chosen as doping elements starting from different precursors of the preparation of the modified films. The films, whose thickness was about $100nm$, were deposited on alumnia substrates supplied with interdigitated electrodes and platinum heater, by the spin coating technique at 3000 rpm, dried at 80 °C and heat treated in air at 600 °C. After deposition, the sensors were mounted onto a TO8 socket and inserted in the test chamber.

Samples of different compounds were introduced into a vial kept at room temperature by a thermostatic tank. Many subsequent measurements were performed, for each sample, by fixing the exposure time and the purging time at 20 minutes. The responses have been acquired with a sampling interval of 32 seconds then acquiring 75 points for each response.

Three gases have been taken under consideration (216 measurements in total): Acetone, Hexanal, and Pentanone in 50% relative humidity (RH) and dry air. For a preliminary analysis these gases in 50% RH.

Two different kinds of analysis have been carried out by using PCA and neural network. The first analysis is purely qualitative and for visualization purposes, project data obtained by the several feature extraction methods previously discussed onto the first two useful principal components.

Principal Component Analysis is usually carried out as a low pass filter, in order to reduce noise in the signal, keeping components corresponding to the first few eigenvectors that capture most of the variance contained in the data set. Usually the transformation is made into 2D or 3D spaces. Let $\mathbf{A}$ be the truncated transformation matrix constituted of the first useful principal components of the correlation matrix of the data set. In the experiments that follow in this paper, the first three principal components from the measurements y_{ij} have been extracted, so the matrix $\mathbf{A}$ is $3 \times n$ and then the observation becomes the 3D vector $x_j = \mathbf{A} \cdot y_j$.

The second analysis is more deep because is based on the classification results of a Radial Basis Function neural network, which is given a pattern composed of the coefficients extracted with a pre-processing method. The training and validation procedure is performed by using the

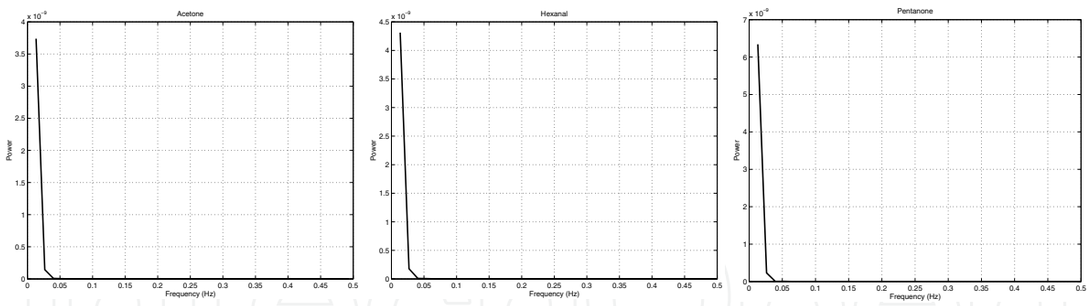

Fig. 3. Power spectra density computed on three different odour responses.

leave-one-out procedure which provides an estimate of the generalization performances of the final classifier.

The RBF network used, creates neurons one at a time. At each iteration the input vector which will result in lowering the network $sum - squared$ error, is used to create a new radial basis neuron. The error of the new network is checked, and if low enough the learning phase is finished. Otherwise the next neuron is added. This procedure is repeated until the error goal is met (0.001), or the maximum number of neurons is reached (i.e. the number of training vectors 215). A spread of 0.8 is used for radial basis functions in order to ensure that more than one neuron can respond to overlapping regions of the input space.

Analysis in the frequency domain has been carried out and figure 3 shows three curves relative to one of the three gases under consideration. The electronic nose responses possess the same frequency domain but different magnitudes for different odors. So an appropriate low pass filter is suitable for feature extraction since the responses have the useful information we need lying in low frequencies, as opposed to noise that is present in high frequencies. Unfortunately, drift also resides in low frequencies and this method carries also this problem in the transformation, but the reduction of the drift is outside the scope of this paper. As introduced in the previous sections, at each level (scale) of signal decomposition, wavelet coefficients are divided by approximation (low frequencies) and details (high frequencies). Also, the coefficients are obtained by convolving the wavelet function and the response curve, thus measuring their correlation degree. The mother wavelet used is the Daubechies family since they guarantee an orthogonal analysis, a necessary condition for feature extraction. After choosing the mother wavelet to use, the next investigation is the level to stop for getting the approximation coefficients of the DWT. The higher the scale the more low frequencies are amplified and high frequencies are cut off. But this is not an infinite process, infact the decomposition level has a lower limit that is the sampling period and a superior limit that is the signal support. The maximum decomposition level of the DWT is the 2-base logarithm of the length of the signal. Since each transient has a length of approximately 80 samples, then the 6th level is appropriate, where $2^6 = 64 < 80$ (the 7th level requires a signal greater than 80 samples).

The graph of the coefficients for one sensor and 3 exposures of the sensor array to the same odor (hexanal) is given in fig. 5 where coefficients up to the 6th decomposition level are shown. The first 13 coefficients on the x-axis shows approximation and the remainings show details. It is interesting to note that the first coefficients of the three curves fall all in the same position as shown by the leftmost patterns (they overlap each other). This may bring to the conclusion that the same order of coefficients related to the same odor are the same. So in this graph the first three order of coefficients can be taken as features to be successively classified by an opportune classifier. As a counter-example, fig. 4 shows coefficients related to

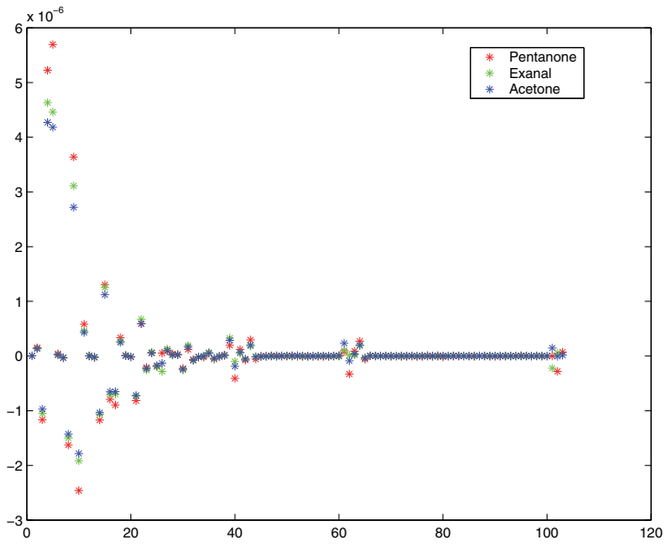

Fig. 4. Coefficients extracted up to the 6-th level of DWT decomposition for three responses of the three considered odour (pentanone, hexanal, and acetone).

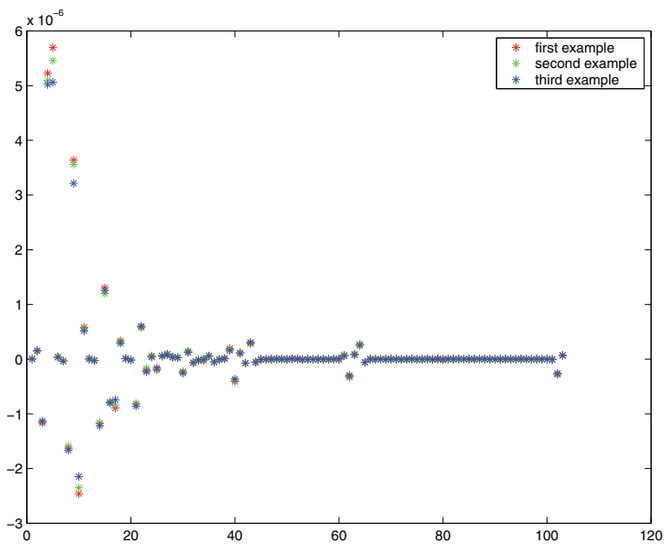

Fig. 5. Coefficients extracted up to the 6-th level of DWT decomposition for three response of the same odour (hexanal).

different odors. However, the first coefficients of the approximation of the three odor curves do not discriminate well since they overlap. The discrimination starts from the third order of coefficient until the sixth, and the scale is larger than the coefficients shown in the figure 5. This states that a number of 6 coefficients is suitable as features and that wavelet transform enlarge the range of the coefficients for different odors while maintaining small the variability of the range coefficients related to the same odor (compare the two figures for the 5th coefficient).
The transient has been analysed in three time parts response: rise time, recovery time and the complete curve (i.e. from the rise time to the next when a new odor is presented). Over all this experiments the extraction of the first 6 coefficients over the complete transient has shown

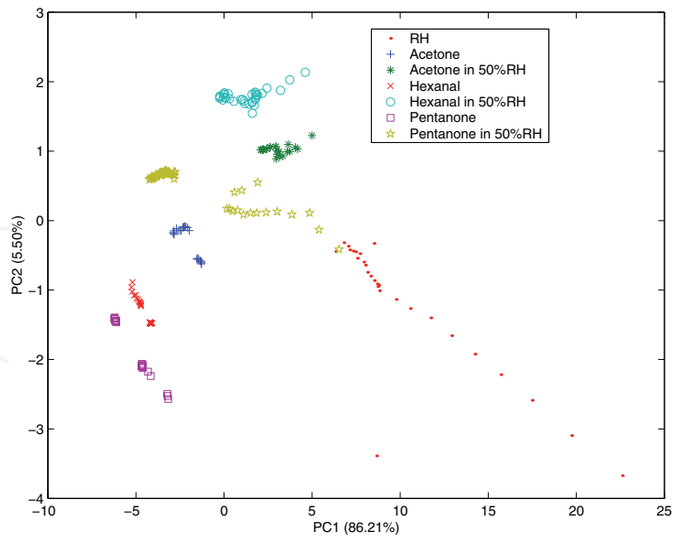

Fig. 6. Principal component analysis done in the wavelet space for the three gases measured in dry and humid air. Each observation has 30 coefficients (features) since for each response of the five sensors, the first six coefficients are extracted (compare the result with the traditional method shown in fig. 7)

better results. However it has been shown that the recovery time is more informative than the rise time, but in general better results are obtained with the complete curve. In fig. 6 is shown the score plot of the first two principal components computed in the wavelet space for visualization. Table 1 gives the classification results with RBF for input pattern of 30 wavelet descriptors.

	(1)	**(2)**	**(3)**	**(4)**	**(5)**	**(6)**	**(7)**
(1)	28	0	0	0	0	0	0
(2)	0	21	0	0	0	0	0
(3)	0	0	25	0	0	0	0
(4)	0	0	0	29	0	0	0
(5)	0	0	0	0	35	0	0
(6)	0	0	0	0	0	22	0
(7)	0	0	0	0	0	0	60

Table 1. Confusion matrix of the wavelet analysis. The total recognition percentage is 100%. (1) Humidity; (2) Acetone; (3) Acetone in 50% RH; (4) Hexanal, (5) Hexanal in 50% RH; (6) Pentanone; (7) Pentanone in 50% RH.

Traditional methods such as the relative, fractional, difference and log parameter, present almost the same behavior for the data under consideration in terms of classification results. Here we report the results of the relative method shown in fig. 7 and the corresponding confusion matrix in table 2 for input patterns to the RBF classifier of 5 coefficients (the number of sensors).

As a comparison, also Fourier descriptors have been tested against wavelet descriptors. Fourier descriptors provide a frequency measure of the curve under consideration without localizing them in the time domain. The Fast Fourier Transform (FFT) is used which allows us to compute very quickly the discrete transformation with a good approximation. The

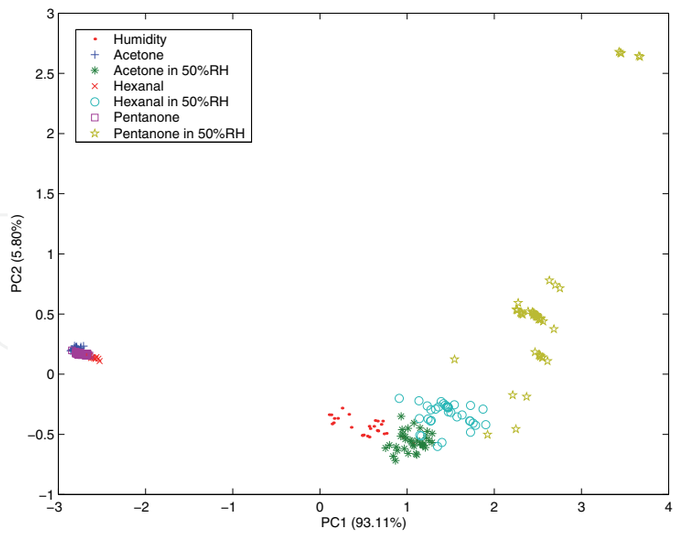

Fig. 7. Result using the traditional method of applying the relative method (I_s / I_0) for the extraction of the features from one response of the sensor and then performing the principal component analysis on the observation space of five elements (one observation from each sensor as opposed to the six extracted with the wavelet analysis).

	(1)	**(2)**	**(3)**	**(4)**	**(5)**	**(6)**	**(7)**
(1)	26	0	2	0	0	0	0
(2)	0	21	0	0	0	0	0
(3)	4	0	16	0	5	0	0
(4)	0	0	0	28	0	1	0
(5)	1	0	1	0	31	0	2
(6)	0	0	0	22	0	0	0
(7)	0	0	0	0	3	0	57

Table 2. Confusion matrix of the relative method feature extraction. The total recognition percentage is 81.36%. (1) Humidity; (2) Acetone; (3) Acetone in 50% RH; (4) Hexanal, (5) Hexanal in 50% RH; (6) Pentanone; (7) Pentanone in 50% RH.

first 10 descriptors have been considered for each curve, since they possess the greatest magnitude and, low frequencies dominate in the response curve. The feature vector pattern is then composed of 50 descriptors, which have been: projected onto the first two principal components for visualization as shown in figure 8 and; given to RBF for discrimination capabilities (table 3).

Integrals and derivatives have also been investigated to benchmark them against the above discussed feature extraction methods.

The aim is the computation of the integral of the f function in the interval $[a, b]$, where a represents the time step of the concentration change in the rise time, and b the end of the recovery time (where $f(t) = 0$). The applied Newton-Cotes method Chapra & Canale (1988) is based on the substitution of the function that represents the transient response with a more simple approximation function:

$$I = \int_a^b f(x)dx \approx \int_a^b f_n(x)dx \tag{27}$$

where $f_n(x)$ is a polynomial function of order n defined as follows:

$$f_n(x) = a_0 + a_1 x + \ldots + a_{n-1} x^{n-1} + a_n x^n \tag{28}$$

The order of the polynomial function determines the accuracy of the method, in our experiments we used the "Simpson's 1/3 Rule" which uses a second order polynomial function.
Simpson's rule finds the area under the parabola which passes through 3 points (the end points and the midpoint, i.e. x_0, x_1, x_2) on a curve. In essence, the rule approximates the curve by a series of parabolic arcs and the area under the parabolas is approximately the area under the curve. The Simpson's rule as well as the other Newton-cotes methods can be applied only if the points are equally spaced. The transient response has been split into 25 intervals where the area is computed as follows:

$$I = (x_2 - x_0)\frac{f(x_0) + 4f(x_1) + f(x_2)}{6}. \tag{29}$$

The observation pattern is composed of five features each one of them describing the area of the corresponding sensor response. Figure 9 shows the PCA plot of the extracted features. The five features are given to the RBF for training and classification with leave-one-out procedure, and the confusion matrix is given in table 4. It is interesting to note that this method produces very informative features as compared with the results obtained with the wavelet descriptors.
Another applied method is the study of the local gradient over the whole transient response. Even in this case the study of the local gradient has been carried out by approximation using the Taylor series. Starting from a first order Taylor series $f(x_{i+1}) = f(x_i) - f'(x_i)(x_{i+1} - x_i)$ we can approximate the derivative in the point x_i as follows:

$$f'(x_i) = \frac{f(x_i) - f(x_{i+1})}{x_{i+1} - x_i}. \tag{30}$$

The mean derivative has been computed over intervals of 10 point samples so then for the whole transient response a number of $(75/10) \approx 7$ features are obtained, leading to 35 features for each observation of the array five sensors. Figure 10 shows the result of mean derivative method by using PCA and in table 5 the confusion matrix of the 7 feature vectors classified by the RBF is given.

	(1)	**(2)**	**(3)**	**(4)**	**(5)**	**(6)**	**(7)**
(1)	28	0	0	0	0	0	0
(2)	0	20	0	0	0	1	0
(3)	0	0	23	0	2	0	0
(4)	0	0	0	28	0	1	0
(5)	1	0	1	0	33	0	0
(6)	0	0	0	0	0	22	0
(7)	0	0	0	0	2	0	58

Table 3. Confusion matrix of the FFT method. The total recognition percentage is 96.36%. (1) Humidity; (2) Acetone; (3) Acetone in 50% RH; (4) Hexanal, (5) Hexanal in 50% RH; (6) Pentanone; (7) Pentanone in 50% RH.

All of the compounds in dry air have shown good results. Only the cluster related to humidity is well defined and separable from others in all the experiments, while hexanal and acetone

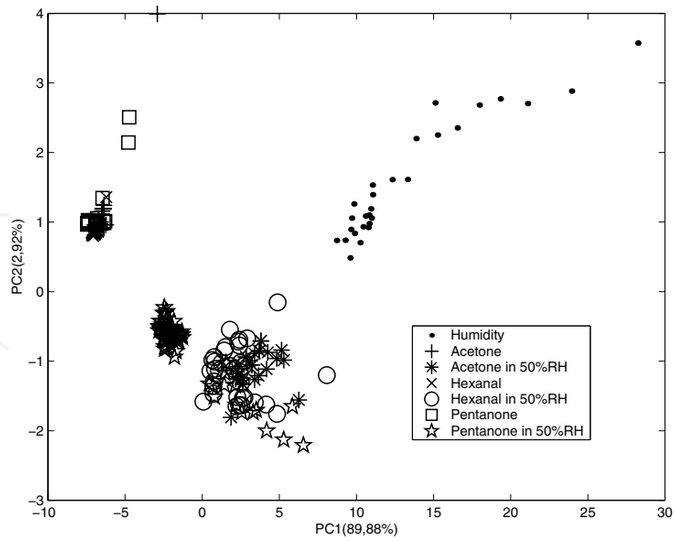

Fig. 8. Principal component analysis done in the Fourier space for the three gases measured in dry and humid air. Each observation has 50 features since for each response of the five sensors, the first ten coefficients are extracted.

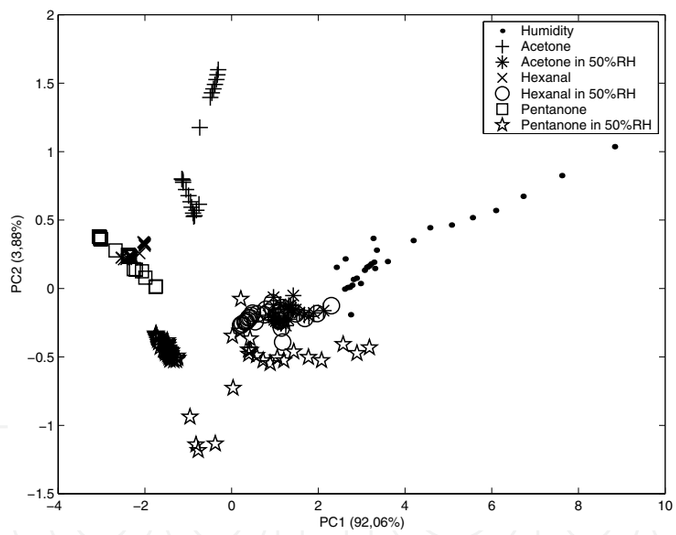

Fig. 9. Principal component analysis with the integration method for gases measured in dry and humid air. Each observation has 5 features corresponding to the areas computed on the responses starting from the release of the aroma in the test chamber.

are mixing up in dry air. Among all the steady-state methods, the difference method have shown better results.

However, when analysed in presence of humidity (50% RH) the performance of the classifier are decreased. It is interesting to note that after inspecting data with PCA, humid compounds and dry compounds are separate from each other. Traditional methods provides poor results in the first two principal dimensions, infact, in the two macro-clusters (dry and humid) the compounds have disordered positions. Hexanal from Pentanone in dry air have correlated

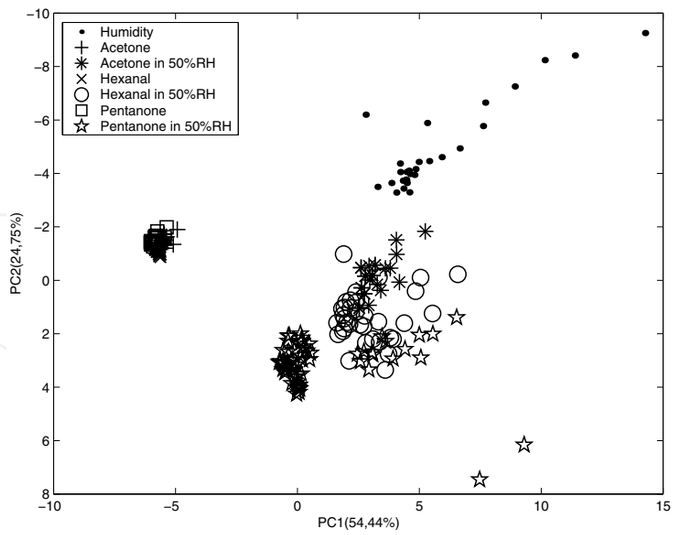

Fig. 10. PCA plot of the features extracted with the derivative method.

	(1)	(2)	(3)	(4)	(5)	(6)	(7)
(1)	28	0	0	0	0	0	0
(2)	0	21	0	0	0	0	0
(3)	0	0	25	0	0	0	0
(4)	0	0	0	29	0	0	0
(5)	0	0	0	0	34	0	1
(6)	0	0	0	0	0	22	0
(7)	0	0	0	0	0	0	60

Table 4. Confusion matrix of the Integration method. The total recognition percentage is 99.54%. (1) Humidity; (2) Acetone; (3) Acetone in 50% RH; (4) Hexanal, (5) Hexanal in 50% RH; (6) Pentanone; (7) Pentanone in 50% RH.

	(1)	(2)	(3)	(4)	(5)	(6)	(7)
(1)	28	0	0	0	0	0	0
(2)	0	20	0	1	0	0	0
(3)	0	0	25	0	0	0	0
(4)	0	0	0	29	0	0	0
(5)	0	0	4	0	29	0	2
(6)	0	1	0	0	0	21	0
(7)	0	0	0	0	2	0	58

Table 5. Confusion matrix of the gradient method. The total recognition percentage is 95.45%. (1) Humidity; (2) Acetone; (3) Acetone in 50% RH; (4) Hexanal, (5) Hexanal in 50% RH; (6) Pentanone; (7) Pentanone in 50% RH.

features, making RBF difficult to classify them correctly. It has been shown that features made only of steady-state information, weakly discriminate classes of odors. Features extracted from the transient response, are more informative but as opposed to traditional steady-state methods, they inherit sensor long term stabilities problems. These are shown with the humidity and Pentanone measurements. The derivative method presents better results with

Pre-processing Method	Recognition rate (%)
Relative	81
Log	81
Difference	83
Fractional	82
Derivative	95.45
Fourier coeff.	96
Integration	99.5
Wavelet coeff.	100

Table 6. Comparison between several feature extraction methods in terms of informative contents contained in each pattern. The results are based on the leave-one-out procedure performed with a RBF neural network.

95% classification rate considering the whole curve analysis. Some of the transient analysis methods have also been investigated for the rise and recovery time. A study of the derivative method restricted to the rise time and recovery time has produced 95% and 93% recognition rates respectively. The integration method have shown results better results both in the PCA space and with RBF classification leading to 99% over the whole response and 96% and 98% for the rise and recovery time respectively. The multiresolution approach with wavelet analysis conducted for the whole response have shown best performance overall methods here presented. In this case, both linear separation and better classification results have been obtained.
Rise time and recovery time parts of the curve gave classification rates of 99% and 100% accuracy respectively.

4.2 Drift counteraction

The micro-sensor array consisted of seven semiconductor metal oxide sensors whose sensing thin film material were pure and doped tin- dioxide SnO_2. Os, Ni, Pt, Pd elements were used as doping elements. The films had been prepared starting from tin tetrachloride, as precursor, with the aim to obtain stabilized SnO_2 solutions The films, whose thickness was 100nm, were deposited on alumina substrates, ($3 \times 3mm^2$) supplied with inter-digitated electrodes and platinum heater, by means of the spin coating technique at 3000 rpm, dried at 80 8C and heat treated in air at 600 8C. After deposition, the sensors had been mounted onto a TO8 socket and inserted in the test chamber. The conditioning of the sensors had been performed by using dry air (flow 100sccm), used also as reference gas for acquiring the baseline current values of the sensors. The device was exposed to three different gases: acetone, hexanal and pentanone in 50% relative humidity (RH). The measurements were performed by fixing the exposure time and the purging time at 20 min. The responses have been acquired with sampling interval of 32 sec. then acquiring 75 points for each response. Further long-term stability of the sensors was tested by performing measurements of baseline current values in dry air over a period of 76 days. At the same time a morphological study on sensor material was performed to reveal poising or ageing during their use by means of the Scanning Electron Microscopy (SEM) images and the X-ray Photoelectron Spectroscopy (XPS) study. As it can be seen in figure 11, it is evident a drifting behavior of all sensors. In this case a drift contamination is more evident for SnO_2-Os based sensor and the pair of identical sensors (SnO_2-Ni and SnO_2-Pd based sensors) show a similar trend in terms of baseline during the whole period

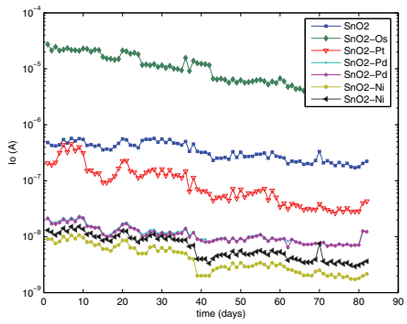

Fig. 11. Effect of drift on the baseline current I_o in dry air over a period of 76 days.

of measurements. The morphological analysis did not reveal effects of the ageing of sensing material while it showed a clear degradation of Ti/Au inter-digitated contacts due to high working temperature Capone et al. (2006). The signal pre-processing method based on

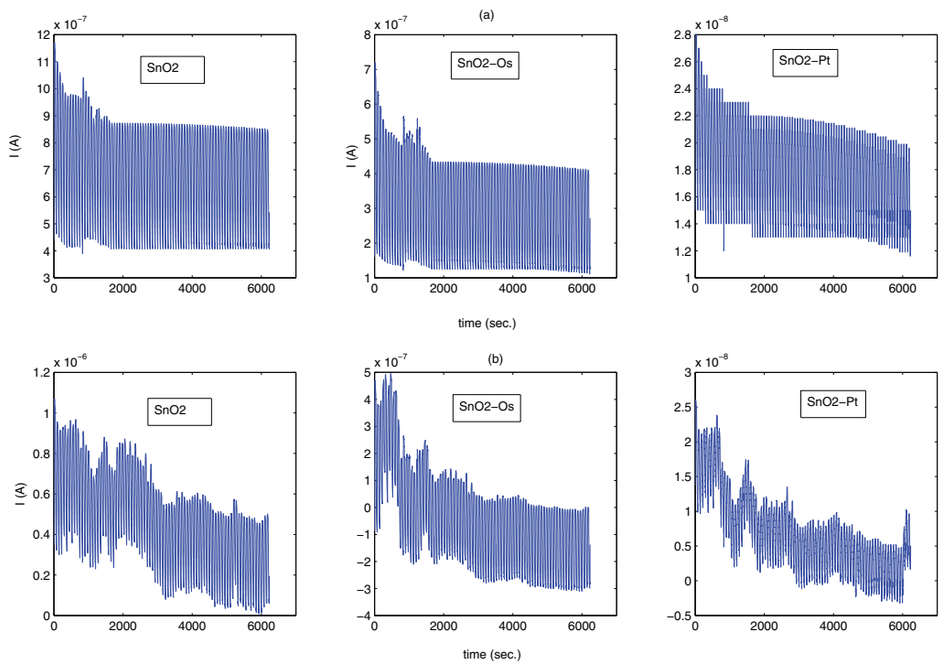

Fig. 12. Example of simulated metal oxide sensor responses to a same odor without drift effect (a) and subjected to drift(b).

DWT was tested on drifting sensor responses, which had been artificially generated in according to the drifting behavior of the sensors previously examined and showed in the fig 11. The drifting signal was obtained by adding the interpolation of sensor's baseline trend to a signal of n repeated cycles of sensor responses (fig. 12). The multilevel wavelet decomposition of these simulated signals was performed by applying iteratively high-pass and low-pass filters. The lowest frequencies influence the deepest levels (in this case the level fixed N), so that the associated approximation coefficients could have drift contamination. In this case it is needed to discard the N-level approximation coefficients containing drift

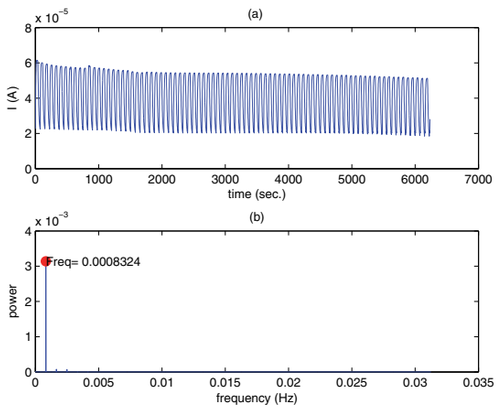

Fig. 13. SnO_2-based sensor response (a). Frequency content of signal via periodogram (b).

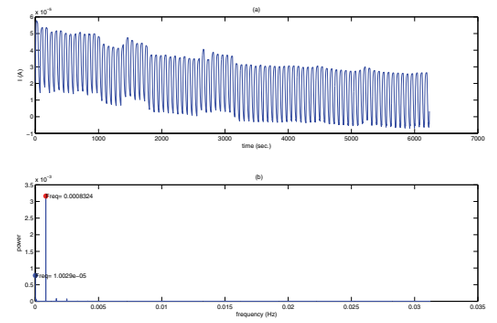

Fig. 14. SnO_2-based sensor response subjected to drift (a). Frequency content of signal via periodogram (b).

contamination. More precisely, each approximation coefficient was fixed to the value of the first approximation coefficient vector element to avoid shifting of the reconstructed signal with respect to the processed one. The wavelet reconstruction was computed by using these changed approximation coefficients and remaining wavelet coefficients from level 1 to N-1. The decomposition level was fixed once analysis in the frequency domain has been carried out to single out the frequency domain of the drifting trend. The figures 13 and 14 show two periodogramms of the SnO_2-based sensor response and the drifting one respectively. The drifting trend frequency component predominates at the scale a which has been gauged by means of the following relationship:

$$F_a = \frac{F_c}{a * \Delta}$$

where a is a scale with $a = 2^N$ (N is the number of decomposition levels), F_c is the center frequency associated to wavelet function, Δ is sampling period and F_a is the pseudo-frequency associated to scale a. The value of F_a must be close to the frequency whose component must be filtered out. The sixth order Daubechies ($db6$) was selected as analyzing wavelet, and the level of wavelet decomposition of the drifting SnO_2-based sensor response was fixed at $N = 6$. The pseudo-frequency F_a associated to scale 2^6 is $3.5511e-04Hz$, so it could filter out the frequency components less than F_a discarding the associated approximation coefficients.

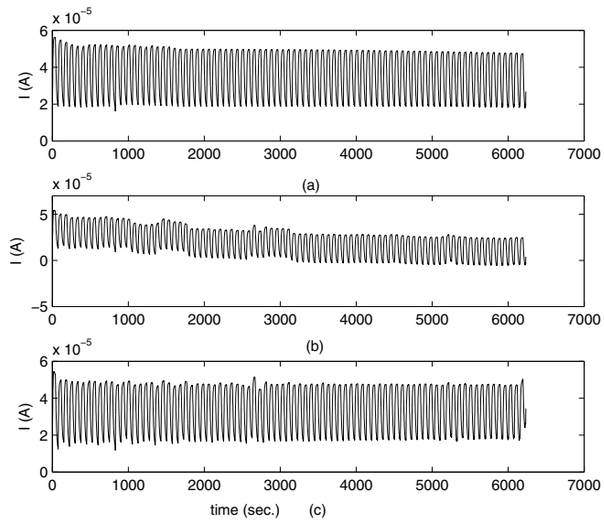

Fig. 15. The original signal (a), the drifting one (b) and DWT-filtered one (c)

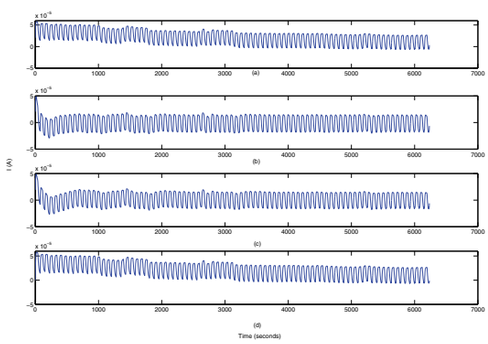

Fig. 16. The drifting signal (a), the Butterworth-filtered one (b), Elliptic-filtered one (c) and FIR-filtered one (d)

Figure 15 shows the filtered signal and tin comparison with the performance of the usual high-pass filters (fig. 16). After pre-processing sensor responses, the relative parameters I_s/I_0 (I_s represents the steady-state current value and I_0 the relative baseline value) were extracted from the drifting and filtered signals. These feature sets was subsequently normalized and analyzed by Principal Component Analysis to visualize the data set. The PCA score plot regarding to the feature set obtained from drifting signals (fig. 17) shows an overlap of the clusters relative to the three gases. A better cluster separation was obtained after the signal pre-processing based on DWT, and in the respective PCA score plot (fig. 18) the three clusters are distinct.

5. Conclusions

The chapter has shown the use of discete wavelet analysis to characterize electronic nose responses from array of gas sensors. The addressed problems were related to signal representation that finds its basis under the signal compression context in order to find compact ways for classification purposes and for denoising under the sensor drift problem.

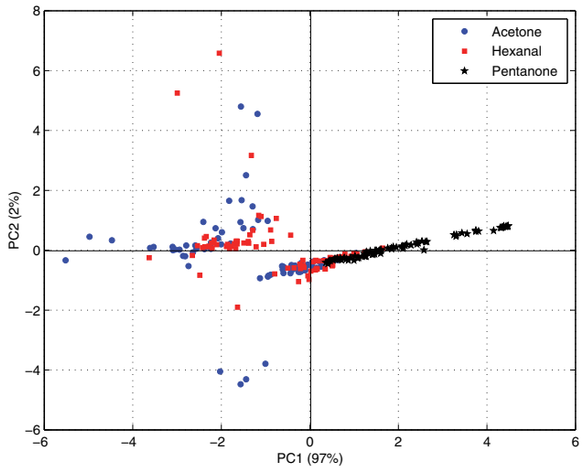

Fig. 17. The PCA score plot of feature sets extracted from drifting sensor responses.

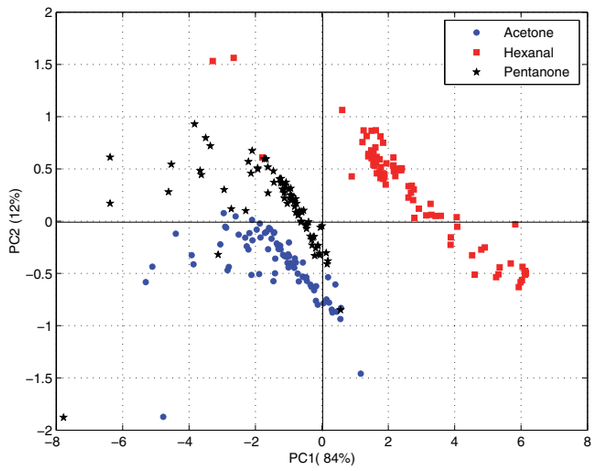

Fig. 18. The PCA score plot of feature sets extracted from DWT-filtered sensor responses.

In the first problem, the study of the transient response in terms of informative content stored in the curve (rise part, recovery part and both) have been investigated. It has been shown with this tool, that the recovery part is more informative than the rise one, but, the use of the whole curve carries better information in terms of discriminability. The feature vector is obtained from the approximation coefficients of multiresolution analysis with wavelet transform and is analysed with principal component analysis and Radial basis Function neural network. Although wavelet transform captures the frequency content of the signal at each decomposition level, it would have been reasonable to make a feature vector composed by maximums approximation coefficients in each level. This performed poorer than the method we used, since a good compression rate and the more discriminative features were obtained with the coeffifients of the highest decomposition level.
The method is compared with the most common techniques of signal processing in the context of electronic nose community. The performed measurements have shown that when we

use the wavelet descriptors the capability of the recognition system to classify three organic compounds improves notably. Table 6 gives the recognition results by using a RBF neural network trained with the features extracted with the considered methods.
This work showed a DWT-based method of signal filtering capable to remove drift effects from the sensor responses and recover the drifting signals to subsequently data analysis. The PCA analysis, employed on features extracted from pre-processed signals showed a clear improvement in the discrimination of the gases with an increase of the distance among the clusters in the principal components space. This signal pre-processing method is enough simple and not time-consuming and the filtered signals are not distorted in comparison with ones obtained by using usual high-pass filters, due to a a more flexible analysis of the signal that wavelet transform allows.

6. References

Acevedo, F., Maldonado, S., Domínguez, E., Narváez, A. & López, F. (2007). Probabilistic support vector machines for multi-class alcohol identification, *Sensors and Actuators B: Chemical* 122(1): 227–235.

Artursson, T., ov ov ov ov, T. E., om om om om, I. L., Mårtensson, P., ostr: om ostr: om, M. S. & Holmberg, M. (2000). Drift correction for gas sensors using multivariate methods, *Journal of Chemometrics* (14): 1–13.

Bakshi, B. R. (1999). Multiscale analysis and modeling using wavelets, *Journal of Chemometrics* 13(3-4): 415–434.

Capone, S., Epifani, M., Francioso, L., Kaciulis, S., Mezzi, A., Siciliano, P. & Taurino, A. M. (2006). Influence of electrodes ageing on the properties of the gas sensors based on sno2, *Sensors and Actuators B: Chemical* 115(1): 396–402.

Chapra, S. & Canale, R. (1988). *Numerical methods for engineers with personal computer applications*, 2nd edn, McGraw-Hill.

Distante, C., Leo, M., Siciliano, P. & Persaud, K. C. (2002). On the study of feature extraction methods for an electronic nose, *Sensors and Actuators B: Chemical* 87(2): 274–288.

Distante, C., Sicilian, P. & Persaud, K. C. (2002). Dynamic cluster recognition with multiple self-organising maps, *Pattern Analysis & Applications* 5: 306–315.

Haugen, J. E., Tomic, O. & Kvaal, K. (2000). A calibration method for handling the temporal drift of solid state gas-sensors, *Anal. Chim. Acta* (407): 23–39.

Huang, D. & Leung, H. (2009). Reconstruction of drifting sensor responses based on papoulis #x2013;gerchberg method, *Sensors Journal, IEEE* 9(5): 595–604.

Leone, A., Distante, C., Ancona, N., Persaud, K., Stella, E. & Siciliano, P. (2005). A powerful method for feature extraction and compression of electronic nose responses, *Sensors and Actuators B: Chemical* 105(2): 378–392.

Loutfi, A., Coradeschi, S., Lilienthal, A. J. & Gonzalez, J. (2009). Gas distribution mapping of multiple odour sources using a mobile robot, *Robotica* 27(02): 311–319.

Mallat, S. (1999). *A wavelet tour of signal processing*, 2nd edn, Academic Press.

Phaisangittisagul, E. & Nagle, H. (2008). Sensor selection for machine olfaction based on transient feature extraction, *Instrumentation and Measurement, IEEE Transactions on* 57(2): 369–378.

Phaisangittisagul, E. & Nagle, H. T. (2010). Predicting odor mixture's responses on machine olfaction sensors, *Sensors and Actuators B: Chemical* In Press, Corrected Proof: –.

Pijolat, C., Riviere, B., Kamionka, M., Viricelle, J. P. & Breuil, P. (2003). Tin dioxide gas sensor as a tool for atmospheric pollution monitoring: Problems and possibilities for improvements, *Journal of Materials Science* 38: 4333–4346.

Rubinstein, R., Bruckstein, A. & Elad, M. (2010). Dictionaries for sparse representation modeling, *Proceedings of the IEEE* 98(6): 1045–1057.

Sisk, B. C. & Lewis, N. S. (2005). Comparison of analytical methods and calibration methods for correction of detector response drift in arrays of carbon black-polymer composite vapor detectors, *Sensors and Actuators B: Chemical* 104(2): 249–268.

Trincavelli, M., Coradeschi, S. & Loutfi, A. (2009). Odour classification system for continuous monitoring applications, *Sensors and Actuators B: Chemical* 139(2): 265–273.

Zuppa, M., Distante, C., Persaud, K. C. & Siciliano, P. (2007). Recovery of drifting sensor responses by means of dwt analysis, *Sensors and Actuators B: Chemical* 120(2): 411–416.

Zuppa, M., Distante, C., Siciliano, P. & Persaud, K. C. (2004). Drift counteraction with multiple self-organising maps for an electronic nose, *Sensors and Actuators B: Chemical* 98(2-3): 305–317.

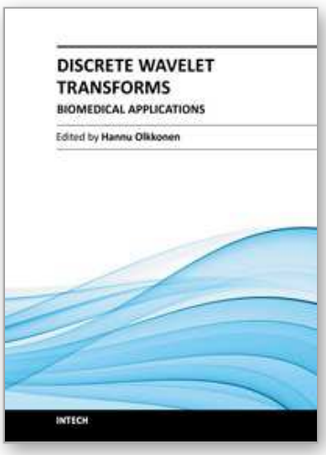

Discrete Wavelet Transforms - Biomedical Applications

Edited by Prof. Hannu Olkkonen

ISBN 978-953-307-654-6
Hard cover, 366 pages
Publisher InTech
Published online 12, September, 2011
Published in print edition September, 2011

The discrete wavelet transform (DWT) algorithms have a firm position in processing of signals in several areas of research and industry. As DWT provides both octave-scale frequency and spatial timing of the analyzed signal, it is constantly used to solve and treat more and more advanced problems. The present book: Discrete Wavelet Transforms - Biomedical Applications reviews the recent progress in discrete wavelet transform algorithms and applications. The book reviews the recent progress in DWT algorithms for biomedical applications. The book covers a wide range of architectures (e.g. lifting, shift invariance, multi-scale analysis) for constructing DWTs. The book chapters are organized into four major parts. Part I describes the progress in implementations of the DWT algorithms in biomedical signal analysis. Applications include compression and filtering of biomedical signals, DWT based selection of salient EEG frequency band, shift invariant DWTs for multiscale analysis and DWT assisted heart sound analysis. Part II addresses speech analysis, modeling and understanding of speech and speaker recognition. Part III focuses biosensor applications such as calibration of enzymatic sensors, multiscale analysis of wireless capsule endoscopy recordings, DWT assisted electronic nose analysis and optical fibre sensor analyses. Finally, Part IV describes DWT algorithms for tools in identification and diagnostics: identification based on hand geometry, identification of species groupings, object detection and tracking, DWT signatures and diagnostics for assessment of ICU agitation-sedation controllers and DWT based diagnostics of power transformers.The chapters of the present book consist of both tutorial and highly advanced material. Therefore, the book is intended to be a reference text for graduate students and researchers to obtain state-of-the-art knowledge on specific applications.

How to reference

In order to correctly reference this scholarly work, feel free to copy and paste the following:

Cosimo Distante, Marco Leo and Krishna C. Persaud (2011). Wavelet Transform for Electronic Nose Signal Analysis, Discrete Wavelet Transforms - Biomedical Applications, Prof. Hannu Olkkonen (Ed.), ISBN: 978-953-307-654-6, InTech, Available from: http://www.intechopen.com/books/discrete-wavelet-transforms-biomedical-applications/wavelet-transform-for-electronic-nose-signal-analysis

INTECH
open science | open minds

InTech Europe
University Campus STeP Ri
Slavka Krautzeka 83/A

InTech China
Unit 405, Office Block, Hotel Equatorial Shanghai
No.65, Yan An Road (West), Shanghai, 200040, China

www.intechopen.com

51000 Rijeka, Croatia
Phone: +385 (51) 770 447
Fax: +385 (51) 686 166
www.intechopen.com

中国上海市延安西路65号上海国际贵都大饭店办公楼405单元
Phone: +86-21-62489820
Fax: +86-21-62489821

IntechOpen

IntechOpen